Journal of Inorganic and Organometallic Polymers and Materials (2023) 33:2721–2731
https://doi.org/10.1007/s10904-023-02713-w

RESEARCH

Impact of Ferromagnetic Ni Substitution on Structural and Magnetic Parameters of $Ba_{0.8}In_{0.2}Fe_{12-x}Ni_xO_{19}$ (x = 0.00–2.00) Hexaferrites

Sana Ullah Asif[1] · Ubaid-ur-Rehman Ghori[2] · Qasim Ali Ranjha[3] · Fahim Ahmed[4] · Gideon F. B. Solre[5] · Ishfaq Ahmad[4] · Fatma A. Ibrahim[6] · Mohamed S. Hamdy[6] · Ebraheem Abdu Musad Saleh[7] · Sayed M. Eldin[8]

Received: 12 April 2023 / Accepted: 10 May 2023 / Published online: 22 May 2023

Abstract

In this work, $Ba_{0.8}In_{0.2}Fe_{12-x}Ni_xO_{19}$ (x = 0.00–2.00) hexaferrites were prepared by the ceramic route, and the effect of ferromagnetic dopant Ni was retrieved on the structure and magnetic properties. Microstructural properties were explored using XRD and SEM. The range of the grain size was between 500 to 2000 nm. In addition to these, micro strain, dislocation density, and porosity were determined. According to the VSM findings, ferromagnetic nickel doping increased the magnetic saturation up to 58.36 emu/g. The coercivity values were observed within a defined range from 5.129 kOe to 5.512 kOe, showing only a slight change. Moreover, the magnetocrystalline anisotropy constant, anisotropy field, and anisotropy parameter were calculated. The results showed that the magnetocrystalline anisotropy constant and anisotropy field both increased up to 0.06308 emu/g.kOe and 1.722 kOe for an increase in doping concentrations and then dropped for x = 2.0. The magnetic moment per formula unit in terms of Bohr magneton was also computed and has an upper limit of 11.603. These results suggest that the synthesized material is a good contender for magnetic applications.

Keywords Magnetic materials · Coercivity · Anisotropy parameters · Bohr magneton · Lattice constant · M-type hexaferrites

1 Introduction

The study of existing materials with varied physical properties enhances the possibilities for creating novel research materials [1–5]. To create new composite materials with highly noticeable electrical and magnetic properties, the research of ferroelectric materials serves as the foundation.

Sana Ullah Asif, Ubaid-ur-Rehman Ghori, Qasim Ali Ranjha, Fahim Ahmed, Gideon F. B. Solre, Ishfaq Ahmad, Fatma A. Ibrahim, Mohamed S. Hamdy, Ebraheem Abdu Musad Saleh, and Sayed M. Eldin have contributed equally to this work.

✉ Sana Ullah Asif
sanaullahasif@gmail.com

✉ Fahim Ahmed
fahim.ahmed@ue.edu.pk

[1] Key Laboratory of LCR Materials and Devices of Yunnan Province, National Center for International Research On Photoelectric and Energy Materials, School of Materials and Energy, Yunnan University, Kunming 650091, People's Republic of China

[2] Department of Industrial & Manufacturing Engineering (RCET), University of Engineering & Technology, Lahore, Pakistan

[3] Department of Mechanical Engineering, RCET Campus, University of Engineering and Technology, Lahore, Pakistan

[4] Department of Physics, Division of Science and Technology, University of Education, Lahore, Pakistan

[5] School of Pharmaceutical Science and Technology, Tianjin University, Tianjin 300072, People's Republic of China

[6] Catalysis Research Group (CRG), Department of Chemistry, College of Science, King Khalid University, P.O. Box 9004, Abha 61413, Saudi Arabia

[7] Department of Chemistry, College of Arts and Sciences, Prince Sattam Bin Abdulaziz University, Wadi Al-Dawasir 11991, Saudi Arabia

[8] Center of Research, Faculty of Engineering, Future University in Egypt, New Cairo 11835, Egypt

Research reveals that adding diamagnetic elements to ferroelectric materials results in the creation of novel functional materials [6–11]. Multiferroics are the name given to such compounds because they have both electrical and magnetic properties. Multiferroics became extremely useful in contemporary sectors of electronics as a result of the development of the interaction of both magnetic and electrical characteristics. Compounds having diverse features, such as strong coercivity, high magneto-crystalline anisotropy, high resistivity, etc., are known as ferrites, a type of ferromagnetic metal oxide [12]. These ferrites are divided structurally into three categories such as hexagonal, spinel, and garnets. Hexagonal ferrites shortly called hexaferrites too have many types depending upon their compositions which include M-type hexaferrites, U-type hexaferrites, W-type hexaferrites, X-type hexaferrites, Y-type hexaferrites, and Z-type hexaferrites [13–18]. Most commonly used ferrites, M-type hexaferrites with the chemical formula $MFe_{12}O_{19}$ (where M = Ba, Sr, Pb) have attracted the interest of many researchers because of their vast applications in electronics especially in ultra-high frequency ranges due to their high saturation magnetization, chemical stability perfection [2, 3, 19]. Due to their numerous uses and outstanding performance-price ratio, barium M-type hexaferrites (BaM) are significant since they account for half of the overall products of magnetic materials created worldwide. They have a wide range of applications as electromagnetic wave absorbers, magnetic storage media, magnetic filters, spintronics, and recording media [20–24]. In addition to their typical magnetic properties researchers are also interested in their utilization of the gigahertz and microwave frequency bands [14]. The magnetocrystalline anisotropy of hexagonal ferrites, which is a result of strong exchange coupling of Fe^{3+} spin at various areas, is tightly correlated with their high coercivity values [25–28].

Previous studies have shown that with partial substitutions of Sr^{2+} or Ba^{2+} and Fe^{3+} ions by several ions, such as La^{3+}, Zn^{2+}, Al^{3+}, Cu^{2+}, Ce^{2+}, Co^{2+}, Ti^{4+}, Mn^{2+}, Mo^{6+}, etc. affect the basic properties of barium hexaferrite [5, 7–10, 29–31]. Atendra et al. prepared the nickel-doped M-type hexaferrites with a chemical reaction method. The magnetic hysteresis curve showed that the material's ferromagnetic behavior was temperature dependent [32]. Makhdoom et al. reported that doping of Ce-Al ions in M-type hexaferrites showed shrinking of iron surroundings at different sites that enhanced the magneto crystalline anisotropy and an increase in coercive forces at different sintering temperatures [33–36]. Khalid et al. reported that the doping of yttrium and cobalt on M-type hexaferrites showed the enhancement of magnetic properties. They observed an increase in coercivity with an increase in the doping concentration of yttrium and decreasing the doping concentration of cobalt. Saturation magnetization first increased and gradually decreased after a sintering temperature of 1250 °C [37]. Furthermore, indium-doped barium hexaferrites were investigated to see the effect of In against Fe and it was observed that magnetic moments decreased as the substitution level rises because the superexchange connections between the magnetic positions both within and outside the sublattices are broken. Due to the weakening of the Fe–O-Fe exchange interaction, the Curie temperature appeared to fall as the concentration of diamagnetic cations increased, which destroyed magnetic order at lower temperatures [18, 38, 39].

In this work, we have reported the impact of ferromagnetic nickel substitution on structural and magnetic parameters of synthesized $Ba_{0.8}In_{0.2}Fe_{12-x}Ni_xO_{19}$ (x = 0.00, 0.50, 1.00, 1.50, 2.00) hexaferrites. The base compound was prepared by considering charge compensation mechanism as it is a unique way to alter properties. Microstructural parameters were calculated using XRD refinement, W–H plot and magnetic properties including the different magnetic anisotropic parameters such as K, H_a, B, were estimated etc. The results showed an increase in the magnetic saturation with increasing doping of ferromagnetic nickel. The coercivity values were found in a specific range showing a small change for different values of concentration (x).

2 Experimental Work

2.1 Sample Preparation

All of the samples of M-type hexaferrite $Ba_{0.8}In_{0.2}Fe_{12-x}Ni_xO_{19}$ (x = 0.00, 0.50, 1.00, 1.50, 2.00) used in this investigation were made using the conventional solid-state reaction method. The starting materials $BaCO_3$, Al_2O_3, In_2O_3, and Fe_2O_3, purchased from Aladdin chemicals and contained a purity level of 99.9% were mixed according to the stoichiometric ratios by using a planetary ball mill, and the sample was ground for 10 h while the components were combined with zirconia balls and ethanol as a medium in nylon jars. To remove any remaining moisture before further processing, the material was removed from the ball mill, dried, and ground. To remove the carbonates, the material was calcined at 1100 °C. After that, it was exposed to a 6-h ball milling process before being dried and powdered once more. Using a vibration mill, the material was further broken down into particles smaller than 90 nm. The material was then sintered for 2 h at a temperature of 1250 °C. The resultant solid solution was pressed into pellets of 12 mm diameter and 1.2 mm thickness for scanning electron microscopy investigation. The pellets underwent another sintering procedure at 900 °C to remove any PVA binder leftover. The generalized chemical equation for the reaction can be as:

$$BaCO_3 + In_2O_3 + Fe_2O_3 + NiO + O_2 \rightarrow Ba_{0.8}In_{0.2}Fe_{12-x}Ni_xO_{19}$$

where x is the amount of Nickel oxide added and can be varied depending on the requirement of the desired material.

2.2 Properties Measurements

An analytical X'Pert Pro X-Ray diffractometer was used to examine the sample's structural makeup. With the use of a HITACHI S-4800 scanning electron microscope, measurements of the structure of the samples were performed utilizing the sample pellets. The sample's magnetic characteristics were then assessed at room temperature using Chinese-made NIM-2000HF magnetic measuring equipment.

3 Results and Discussions

3.1 Structural Analysis

A crucial tool for examining the properties of the material is structural analysis [40, 41]. The X-ray diffraction analysis of $Ba_{0.8}In_{0.2}Fe_{12-x}Ni_xO_{19}$ (x = 0.00, 0.50, 1.00, 1.50, 2.00) was carried out in a range (20–80) degrees throughout the data gathering by using an x-ray diffractometer. The XRD pattern matched JCPDS card #43-0002 and indicated that the hard phase of barium ferrite had formed [42]. The formation of a magnetoplumbite structure with a space group of P63/MMC (No. 194) was confirmed by the observed diffraction pattern [43]. Every diffraction pattern exhibited an M-type or magnetoplumbite structure. No additional peaks related to other phases were found except Fe_2O_3. The high peak intensity indicated that the samples seemed to be of excellent quality and had a good crystalline phase. Figure 1(a-c) shows the XRD patterns of $Ba_{0.8}In_{0.2}Fe_{12-x}Ni_xO_{19}$ (x = 0.00, 0.50, 1.00, 1.50, 2.00) hexaferrites along with lattice parameters and expected crystal structure obtained through structural refinement.

The lattice parameters were calculated by refinement of the XRD patterns of $Ba_{0.8}In_{0.2}Fe_{12-x}Ni_xO_{19}$ (x = 0.00, 0.50, 1.00, 1.50, 2.00) by using Celref software based on the five iron sites [41, 44–46]. The variation in intensity peaks could be well observed as a result of doping. Table 1 reveals the overall lattice parameters determined for the $Ba_{0.8}In_{0.2}Fe_{12-x}Ni_xO_{19}$ (x = 0.00, 0.50, 1.00, 1.50, 2.00) hexaferrites. "Fe" generally possesses five uneven sites, including three octahedral sites (2a, 12 k, 4f2), one tetrahedral site (4f1), and a trigonal bipyramidal site (2b) [47, 48]. Figure 2a shows the volume of the samples along the c/a ratio for the synthesized samples. The c/a value ranging between (3.8781 to 3.9629) as indicated in Table 1 and less than 3.98 as reported earlier could also serve as confirmation of the formation of M-type hexaferrites [49].

It could be seen that 'a' initially increased with increasing doping levels but declined at the highest levels of doping.

Table 1 Refined Lattice parameters of $Ba_{0.8}In_{0.2}Fe_{12-x}Ni_xO_{19}$ (x = 0.00, 0.50, 1.00, 1.50, 2.00) hexaferrites

x	*a* (Å)	*c* (Å)	c/a	*V* (Å)^3	χ^2
0.0	5.8958	23.0907	3.9165	695.0891	1.06
0.5	5.9294	22.9950	3.8781	700.1205	1.07
1.0	5.9535	23.0712	3.8752	708.1623	1.10
1.5	5.8888	23.1666	3.9340	695.7103	1.14
2.0	5.8495	23.1812	3.9629	686.8964	1.11

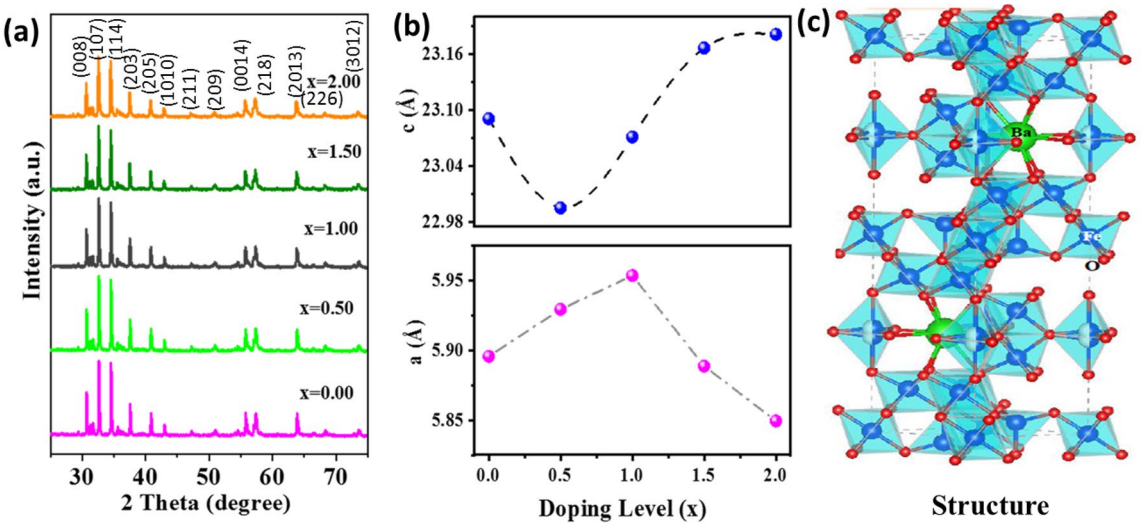

Fig. 1 **a** XRD patterns of $Ba_{0.8}In_{0.2}Fe_{12-x}Ni_xO_{19}$ (x = 0.00, 0.50, 1.00, 1.50, 2.00) hexaferrites. **b** Lattice parameters a and c vs doping level (x). **c** Expected crystal structure based on refinement results

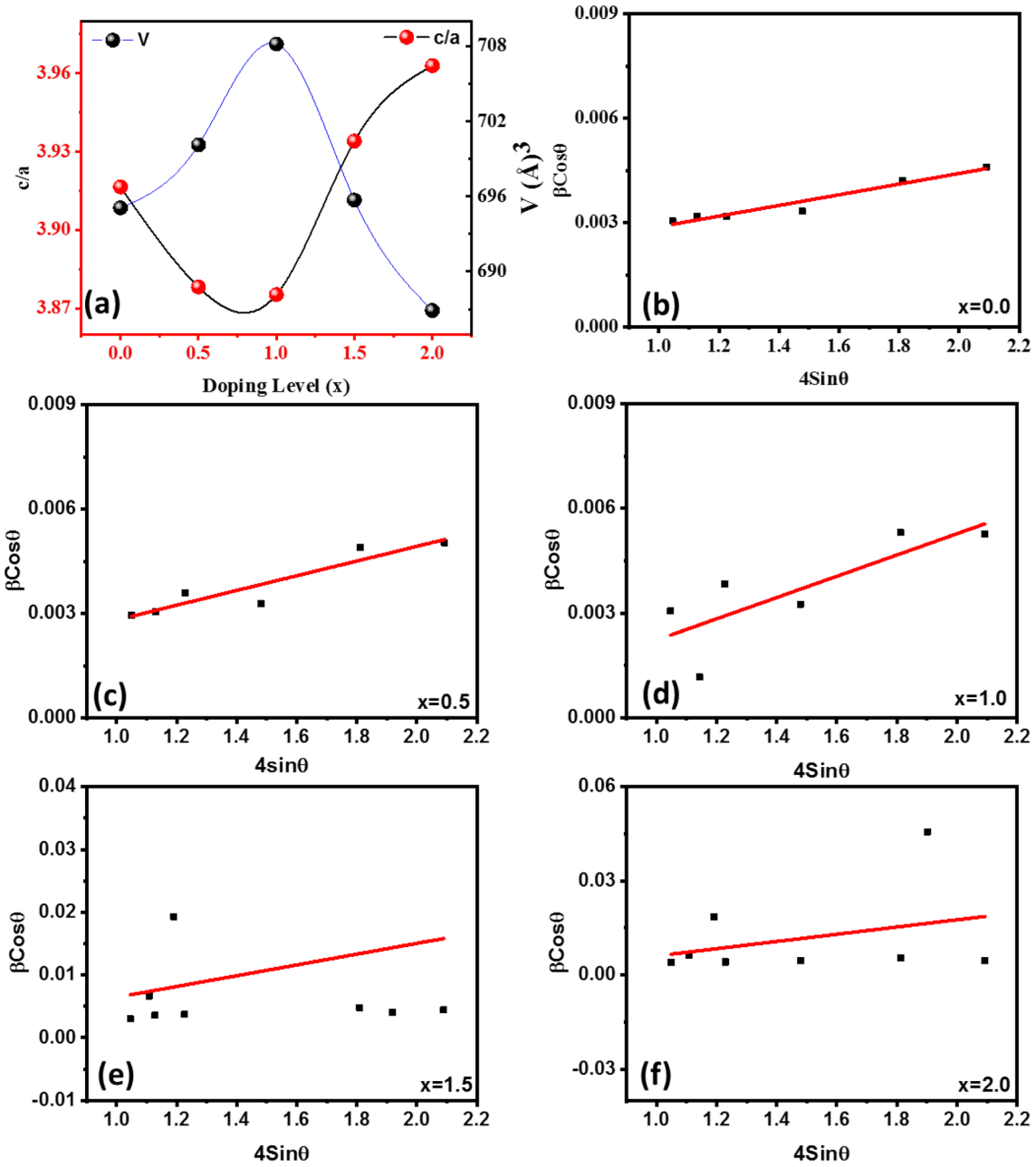

Fig. 2 **a** c/a ratio and volume (V) vs different doing levels of $Ba_{0.8}In_{0.2}Fe_{12-x}Ni_xO_{19}$ hexaferrites. **b–f** W–H plots for the $Ba_{0.8}In_{0.2}Fe_{12-x}Ni_xO_{19}$ hexaferrites

Additionally, for the maximal doping level, 'c' showed a drop earlier and then a rise. As a result, the parameter changes suggested that as the quantity of doping is increased, the lattice initially contracted before expanding towards the c-axis. These patterns could portend significant developments in the present magnetic material system [50]. Additionally, the difference in the ionic radii of the dopants (Indium and Nickel) in the synthesized samples was what caused the shift in lattice characteristics. The non-linear dependence in lattice parameters with increasing Ni^{2+} content in M-type $Ba_{0.8}In_{0.2}Fe_{12-x}Ni_xO_{19}$ hexaferrites could be attributed to the competition between the substitution of Ni^{2+} for Fe^{3+} and the distortion of the crystal structure due to the size mismatch between the dopant and host ions. The ionic radii of the Fe^{3+} and Ni^{2+} ions vary depending on the coordination number and oxidation state of the ion. For the oxygen coordination number of 6, the ionic radii of Fe^{3+} and Ni^{2+} are approximately 0.645 Å and 0.690 Å, respectively. For the oxygen coordination number of 12, which is typical for M-type hexaferrite, the ionic radii of Fe^{3+} and

Ni^{2+} are approximately 0.645 Å and 0.780 Å, respectively. When Ni^{2+} is substituted for Fe^{3+} in the lattice, the larger size of the Ni^{2+} ion could distort the crystal structure due to the size mismatch with the neighboring Fe^{3+} ions. This distortion can cause changes in the lattice parameters a and c, which describe the lengths of the crystallographic axes along the hexagonal plane and the c-axis perpendicular to the plane, respectively. Micro strains play a key role in the discussion of deformation in the crystal. Furthermore, Williamson Hall (W–H) method is employed to calculate strain among the crystallites. Figure 2b–f showed the W–H plots of the M-type $Ba_{0.8}In_{0.2}Fe_{12-x}Ni_xO_{19}$ hexaferrites, along with the micro strain in Table 2. The micro strain showed an increase with increasing content of Ni, well-linked to the deformation due difference in the ionic sizes of the dopant and host cation in the synthesized sample [51–53]. Lattice is usually distorted to accommodate the dopant atom in the crystal lattice.

Additional microstructural variables of the synthesized samples, including average crystallite size D, micro strain, bulk density d_b, X-ray density d_x, and porosity P, were also investigated [54]. The average crystallite size was calculated using the well-known Scherrer formula and the following formulas were used to determine the other parameters, d_b, d_x, and P [33, 55, 56].

$$D = \frac{K\lambda}{\beta Cos\theta} \tag{1}$$

$$d_x = \frac{ZM_w}{N_A V} \tag{2}$$

$$d_b = \frac{m}{\pi r^2 h} \tag{3}$$

$$P = \left(1 - \frac{d_b}{d_x}\right) \times 100 \tag{4}$$

where k = 0.9, λ = 1.5409 Å, β refers to full-width half maximum (FWHM), the diffraction angle is referred to as θ, M_{wt} represents the molar weight and 'r' represents the radius, and 'h' represents the thickness of the pellet. The calculated parameters are shown in Table 2.

To determine the vacant spaces, present in the material, dislocation density (δ) was calculated from crystallite size by the equation given below [57].

$$\delta = 1/D^2 \tag{5}$$

Most often, smaller crystallites merging into larger ones and clusters creating new grain boundaries were the principal causes of dislocation. The plot of estimated microstructural parameters against different doping levels (x) was shown in Fig. 3(a-b). Both densities showed a decrease for the starting values, but when the concentration of the dopants was increased, both started increasing.

The trends could be further explained based on the M_{wt} of the samples. The higher X-ray density results implied that the materials contain pores. While variations in dislocation density (**δ**) and porosity 'P' may also be closely related to variations in oxide vacancies [40, 58]. In general, these variations in micro parameters may lead to a change in the material's magnetic properties.

3.2 Morphological Analysis

Samples of $Ba_{0.8}In_{0.2}Fe_{12-x}Ni_xO_{19}$ (x = 0.00, 0.50, 1.00, 1.50, 2.00) were subjected to scanning electron microscopy to ascertain the creation of shape and the existence of secondary phases. The findings demonstrated that the material lacked any secondary phases and that the particles' hexagonal shape could be seen in the micrographs. The sample's uniform and homogeneous distribution was further confirmed by the SEM images in Fig. 4. The loss of the PVA binder was seen in the photographs as pores. Doping may impact the form of the hexaferrites instead of their size because the addition of dopants did not cause appreciable changes in grain size. The shape of the particles was observed to be spherical. However, some agglomeration could be well observed with increasing doping levels as well. Furthermore, the morphological images demonstrated that pure hexaferrites were successfully formed. The range of the grain size was between 500 to 2000 nm.

Table 2 Microstructural parameters average crystallite size D, Micro strain (ε), bulk density d_b, X-ray density d_x, dislocation density (δ), and porosity P of $Ba_{0.8}In_{0.2}Fe_{12-x}Ni_xO_{19}$ (x = 0.00, 0.50, 1.00, 1.50, 2.00) hexaferrites

(x)	D(nm)	ε strain	d_x(g cm^{-3})	d_b(g cm^{-3})	P (%)	δ ($1/nm^2 \times 10^{-4}$)
0.0	50.86	0.0015	5.29	4.47	15.3	3.86
0.5	51.77	0.0021	5.25	4.44	15.4	3.73
1.0	49.43	0.0030	5.20	4.38	15.7	4.09
1.5	53.58	0.0086	5.30	4.50	15.1	3.48
2.0	48.11	0.0113	5.38	4.53	15.6	4.31

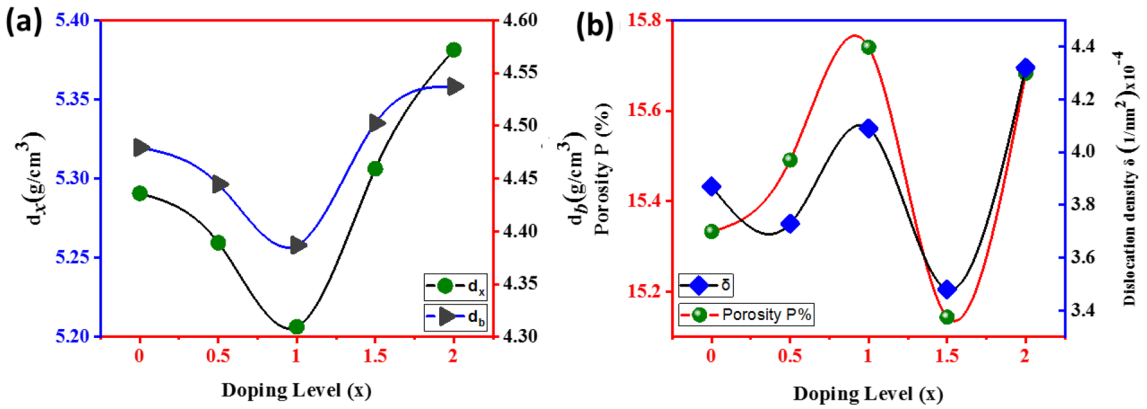

Fig. 3 **a** X-ray density, and Bulk density variation with doping level (x). **b** Porosity and dislocation density for different doping concentrations of $Ba_{0.8}In_{0.2}Fe_{12-x}Ni_xO_{19}$

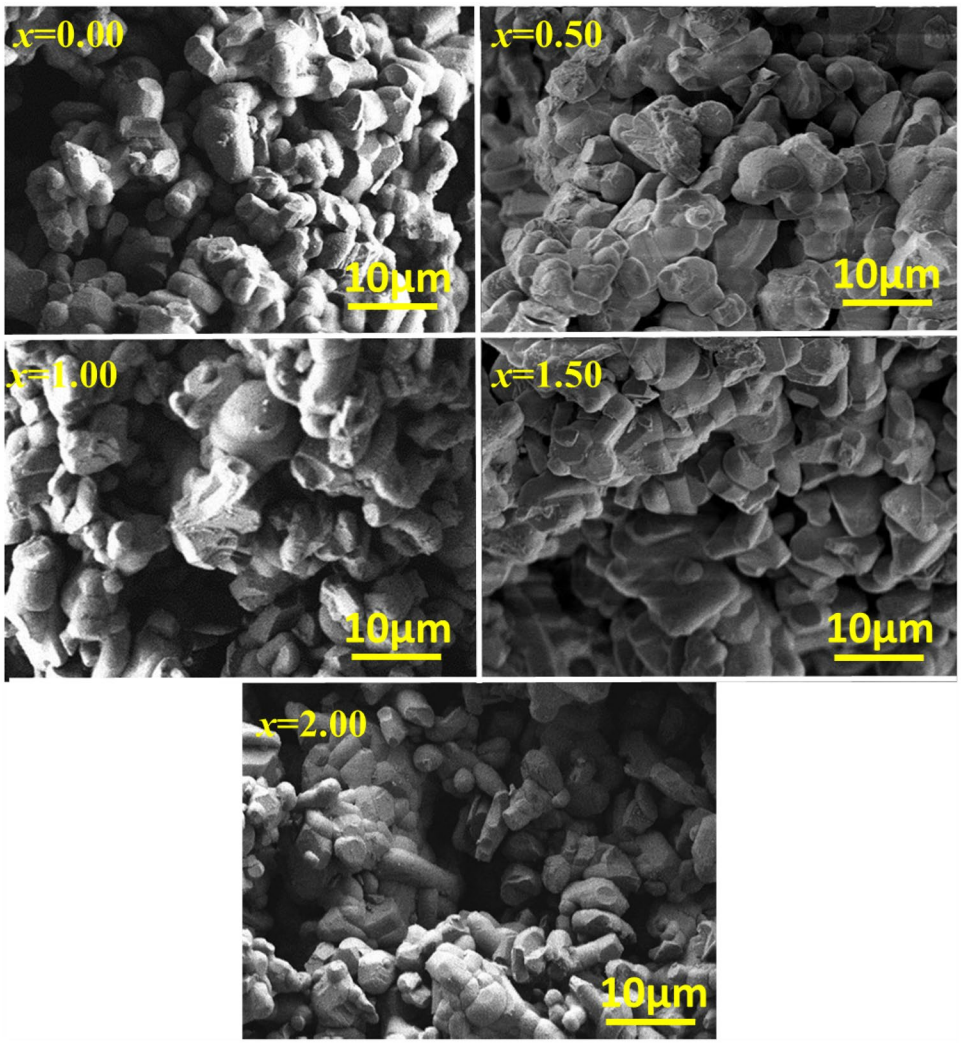

Fig. 4 SEM images of $Ba_{0.8}In_{0.2}Fe_{12-x}Ni_xO_{19}$ (x = 0.00, 0.50, 1.00, 1.50, 2.00) hexaferrites

4 Magnetic properties

Magnetic characteristics of $Ba_{0.8}In_{0.2}Fe_{12-x}Ni_xO_{19}$ (x = 0.00, 0.50, 1.00, 1.50, 2.00) were investigated using applied magnetic fields of about 30 kOe. The combined M-H loops of all samples are also displayed in Fig. 5 showing that M_s increased for the doping concentration till x = 1.5 but then decreased for the dopants at x = 2.0. The magnetic parameters including magnetic saturation (M_s), coercivity (H_c), remanence (M_r), crystalline anisotropic constant (K) in terms of magnetic susceptibility, the magnetic moment per formula unit (m_B), and anisotropy field (H_a), are presented in Table 3. Parent compound $Ba_{0.8}In_{0.2}Fe_{12-x}Ni_xO_{19}$ (x = 0.00) was found to have a coercivity value of H_c of 5.129 kOe and a magnetic saturation M_s value of 48.01 emu/g. The results could be fairly comparable to those for M-type hexaferrites that have already been published [5, 28, 59–62]. Moreover, a little variance in the parent composition findings may be directly related to the diversity in material synthesis techniques.

M_s and H_c values for the synthesized samples $Ba_{0.8}In_{0.2}Fe_{12-x}Ni_xO_{19}$ (x = 0.00, 0.50, 1.00, 1.50, 2.00) increased as the doping level increased. From 0.0 to 1.5, a maximum value of 58.32 emu/g was observed for M_s, while the H_c displayed a minor change and its highest value of 5.512 kOe was observed at concentration x = 1.5 and subsequently started to decline at x = 2.0.

The changing trend in the values of M_s and H_c after the introduction of dopants could be well linked to the weakening of octahedral and tetrahedral superexchange mechanisms [63]. Furthermore, the incorporation of diamagnetic In^{2+} against Ba^{2+} and ferromagnetic Ni against Fe^{3+} may lead to an increase in saturation magnetization M_s by making iron ions unbalanced at 2a sites, producing a nonlinear ferromagnetic arrangement.

Furthermore, the difference between the ionic radii of the dopants and the host atoms creates spaces between magnetic ions and affects the superexchange interaction [3]. The basic building block of the M-type hexaferrite crystal is a cation–anion cluster in which Fe^{3+} ions occupy the interstitial sites between the octahedrons. Figure 6(a,b) showed the variation of different magnetic parameters against different doping levels of $Ba_{0.8}In_{0.2}Fe_{12-x}Ni_xO_{19}$ hexaferrites.

Normally hexaferrites have five nonequivalent sites, 2a,2b, and 12 k spin up while 4f1 and 4f2 spin down. Introducing the Ni in the iron sublattice increased the superexchange interaction causing an increase in magnetization. Usually, Ni prefers to occupy 2a and 12 k sites by disturbing the upward spins of Fe ions, causing a large increase in magnetization and a smaller change in coercivity as well. Another confirmation for the single domain structure of the synthesized material was the M_r/M_s ratio observed to be greater than 0.5 [64]. These results could make the material more useful in magnetic applications such as magnetic filters, recording media, spintronics, etc. The magnetic moment per formula unit in terms of Bohr magneton was also calculated as [65]:

$$m_B = \frac{Mw \times Ms}{5585} \tag{5}$$

Furthermore, magnetocrystalline anisotropy constant K was also determined and shown in Table 3. The charge compensation mechanism that results from the difference of ionic radii, caused the trends of K to match with the M_s and H_c values, which is another important component that

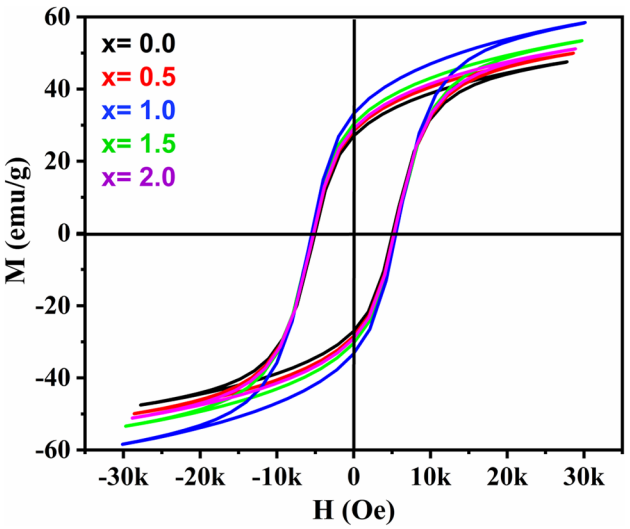

Fig. 5 Combined magnetic loops of $Ba_{0.8}In_{0.2}Fe_{12-x}Ni_xO_{19}$ (x = 0.00, 0.50, 1.00, 1.50, 2.00)

Table 3 Magnetic parameters saturation magnetization (M_s), Remanence magnetization (M_r), Coercivity (H_c), M_r/M_s Ratio, Magnetic anisotropy constant (K) and magnetic moment per formula unit (m_B), and Anisotropy Field (H_a) obtained by analysis of M-H loops

x	M_s (emu g^{-1})	M_r (emu g^{-1})	M_r/M_s	H_c (kOe)	K (emug^{-1}kOe)	m_B (μ_B)	B	H_a (kOe)
0.0	48.01	26.92	0.560	5.129	0.04832	9.516	171,236.4	1.603
0.5	50.23	28.13	0.561	5.292	0.05216	9.968	182,293.1	1.654
1.0	53.53	31.06	0.580	5.446	0.05720	10.636	193,057.1	1.702
1.5	58.32	33.28	0.570	5.512	0.06308	11.603	197,764.8	1.722
2.0	51.20	28.97	0.565	5.25	0.05274	10.200	179,411.1	1.640

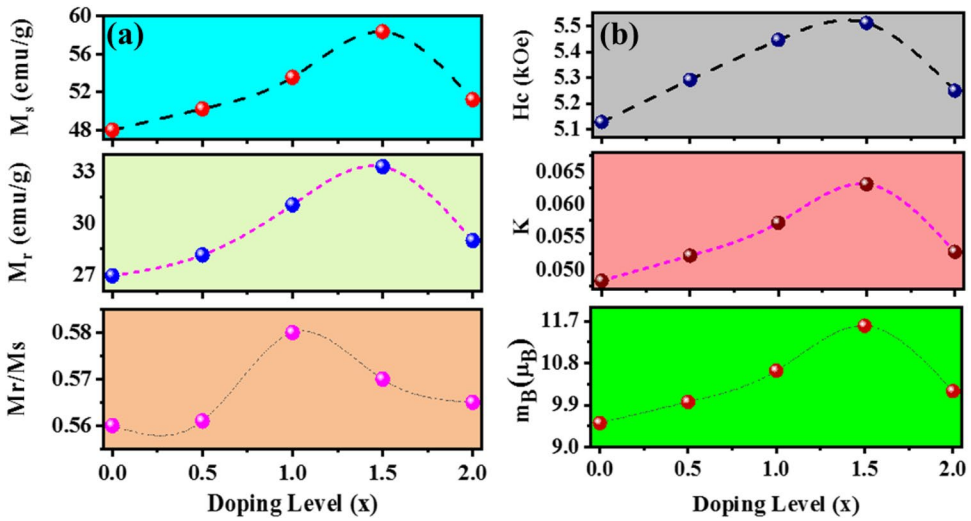

Fig. 6 **a** Variance in M_s, M_r, M_r/M_s vs doping level (x). **b** Variation in H, m_B, and K for different doping levels in $Ba_{0.8}In_{0.2}Fe_{12-x}Ni_xO_{19}$ hexaferrites

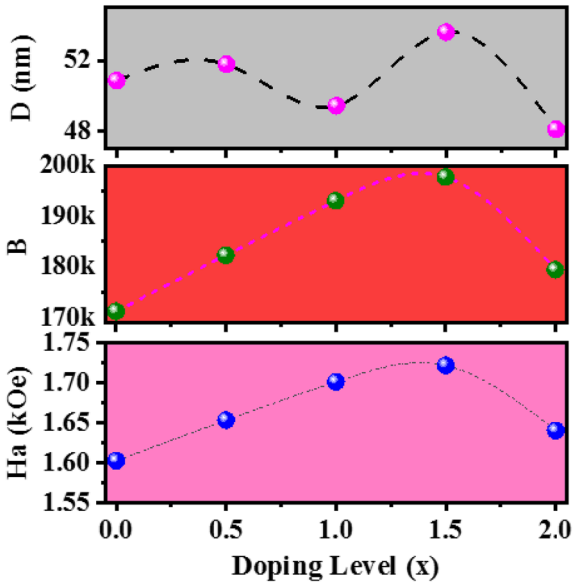

Fig. 7 Variance in anisotropy parameter B, crystallite size D and magnetic anisotropic field vs doping level (x) in $Ba_{0.8}In_{0.2}Fe_{12-x}Ni_xO_{19}$ hexaferrites

influences the characteristics. The anisotropy field (H_a) and anisotropy parameter (B) were also calculated from magnetic parameters as [59]:

$$H_a = \frac{2K}{\mu_\circ M_s} \tag{6}$$

$$B = \frac{4K^2}{15{\mu_\circ}^2{M_s}^2} \tag{7}$$

$$K = \frac{M_s Hc}{5096} \tag{8}$$

where μ_o is the permeability of the vacuum, K is the magneto-crystalline anisotropic constant. Anisotropy parameter B instigates from the resistance of magnetocrystalline anisotropy on domain wall rotation. Figure 7 showed the variation in H_a and B for different doping levels of $Ba_{0.8}In_{0.2}Fe_{12-x}Ni_xO_{19}$ hexaferrites.

The results show that K and H_a both increase for an increase in doping concentrations and then dropped for x = 2.0. Overall Magnetic saturation showed a significant increase with no significant change in coercivity values. Crystallite size also showed a minor change along with other parameters. Furthermore, results suggest that the material has a significant competitor for use in magnetic applications.

5 Conclusions

In this work, M-type hexaferrites $Ba_{0.8}In_{0.2}Fe_{12-x}Ni_xO_{19}$ (x = 0.00–2.00) were synthesized and microstructure was analyzed from the X-ray diffraction data. Lattice constant 'a' was increased from 5.8958 to 5.9535 nm then decreased to 5.8495 but 'c' decreased from 23.0907 to 22.9950 nm, then increased to 23.1812. Morphology showed a uniform and homogenous distribution of particles, with grain sizes ranging from 500 to 2000 nm. W–H plots showed that micro strains were increased upon the introduction of dopants in the crystal lattice. VSM results showed that Magnetic saturation increased from 48.01 to 58.32 $emug^{-1}$, and the coercivity values remained relatively confined in a range. The highest value observed for different magnetic parameters, such as magnetocrystalline anisotropy constant was 0.06308 $emug^{-1}$kOe, anisotropy field was 1.722 kOe, and magnetic

moment per formula unit was observed 11.603μ_B. Overall, this study provides valuable insights for future research and development for magnetic applications.

Acknowledgements The authors are thankful to the Deanship of Scientific Research at King Khalid University for funding this work through a large group Research Project under grant number RGP2/236/44.

Author Contributions All the authors contributed equally to this work. SUA, and FA, conceived the idea. IA and synthesized material, SUA, FA, FI, GFBS, EAMS, and MSH analyzed the data. QA, SME, and UG, formatted the initial draft. The work is a part of IA thesis. The manuscript was written through the contributions of all authors. All authors have approved the final version of the manuscript.

Funding This work was supported by Deanship of Scientific Research, King Khalid University (Grant No. RGP2/236/44)

Data Availability Data is available on request from authors.

Declarations

Competing interests The authors declare that they have no known competing financial interests or personal relationships that could have appeared to influence the work reported in this paper.

References

1. O. Ramanjaneyulu, N. Suresh Kumar, D. Baba Basha, K. Chandra Babu Naidu, Structural, thermal, magnetic, and electrical properties of Ba1−xCuxFe12O19 (x = 0.2–0.8) nanoparticles. J. Mater. Sci. Mater. Electron. **34**(5), 449 (2023)
2. D. Baba Basha, N. Suresh Kumar, K. Chandra Babu Naidu, G. Ranjith Kumar, Structural, electrical, and magnetic properties of nano Sr1−XLaXFe12O19 (X = 0.2–0.8). Sci. Rep. **12**(1), 12723 (2022)
3. M.R. Rehman, M.A. Akram, I.H. Gul, Improved Electrical Properties of Strontium Hexaferrite Nanoparticles by Co2+ Substitutions. ACS Omega **7**(48), 43432–43439 (2022)
4. M. Suganya, S. Anand, D. Mani, M.C. Vu, S. Muniyappan, K.M. Racik, S. Nandhini, J.K. Kumar, Fabrication of novel M-Type cobalt doped barium hexaferrite nanoplatelets/graphitic carbon nitride composite for efficient supercapacitor applications. Synth. Met. **295**, 117341 (2023)
5. A. Trukhanov, V. Turchenko, I. Bobrikov, S. Trukhanov, I. Kazakevich, A. Balagurov, Crystal structure and magnetic properties of the BaFe12− xAlxO19 (x= 0.1–12) solid solutions. J. Magn. Magn. Mater. **393**, 253–259 (2015)
6. R. Cherrington, J. Liang, Materials and deposition processes for multifunctionality, in *Design and Manufacture of Plastic Components for Multifunctionality*. ed. by V. Goodship, B. Middleton, R. Cherrington (William Andrew Publishing, Oxford, 2016), pp.19–51
7. M.A. Malana, R.B. Qureshi, M.N. Ashiq, M.F. Ehsan, Synthesis, structural, magnetic and dielectric characterizations of molybdenum doped calcium strontium M-type hexaferrites. Ceram. Int. **42**(2), 2686–2692 (2016)
8. Z. Mosleh, P. Kameli, A. Poorbaferani, M. Ranjbar, H. Salamati, Structural, magnetic and microwave absorption properties of Ce-doped barium hexaferrite. J. Magn. Magn. Mater. **397**, 101–107 (2016)
9. S.B. Narang, P. Kaur, S. Bahel, C. Singh, Microwave characterization of Co–Ti substituted barium hexagonal ferrites in X-band. J. Magn. Magn. Mater. **405**, 17–21 (2016)
10. S. Vadivelan, N.V. Jaya, Investigation of magnetic and structural properties of copper substituted barium ferrite powder particles via co-precipitation method. Results Phys. **6**, 843–850 (2016)
11. S.U. Asif, Q.A. Ranjha, U.-u-R. Ghori, M. Nisa, M.S. Ahmad, M. Bukhari, N. Jabeen, A. Hussain, N. Hassan, F. Ahmed, Exploring the structural and magnetic trends in Ba0.9Sm0.1Fe12−xAlxO19 M-type hexaferrites. Phys. Scr. **98**(1), 5836 (2023)
12. O. Kitakami, K. Goto, T. Sakurai, A study of the magnetic domains of isolated fine particles of Ba ferrite. Jpn. J. Appl. Phys. **27**(12R), 2274 (1988)
13. V.P. Singh, G. Kumar, R. Kotnala, J. Shah, S. Sharma, K. Daya, K.M. Batoo, M. Singh, Remarkable magnetization with ultra-low loss BaGdxFe12− xO19 nanohexaferrites for applications up to C-band. J. Magn. Magn. Mater. **378**, 478–484 (2015)
14. R.C. Pullar, Hexagonal ferrites: a review of the synthesis, properties and applications of hexaferrite ceramics. Prog. Mater. Sci. **57**(7), 1191–1334 (2012)
15. M. Suganya, J.K. Kumar, S. Anand, K.M. Racik, S. Muthupandi, S. Muniyappan, Electrochemical studies of novel X-Type barium hexaferrite nanoplatelets for supercapacitor applications. J. Supercond. Nov. Magn. **35**(3), 915–923 (2022)
16. S. Anand, S. Muniyappan, K.M. Racik, A. Manikandan, D. Mani, S. Nandhini, P. Karuppasamy, M.S. Pandian, P. Ramasamy, N.K. Chandar, Fabrication of binary to quaternary PVDF based flexible composite films and ultrathin sandwich structured quaternary PVDF/CB/g-C3N4/BaFe11.5Al0.5O19 composite films for efficient EMI shielding performance. Synth. Met. **291**, 199 (2022)
17. M. Suganya, J.K. Kumar, S. Anand, K.M. Racik, S. Muthupandi, S. Muniyappan, S. Nandhini, Synthesis and electrochemical investigation of Z-type barium hexaferrite nanoplatelets. Inorg. Chem. Commun. **139**, 109412 (2022)
18. Y. Yang, F. Wang, J. Shao, D. Huang, H. He, A. Trukhanov, S. Trukhanov, Influence of Nd-NbZn co-substitution on structural, spectral and magnetic properties of M-type calcium-strontium hexaferrites Ca0.4Sr0.6−xNdxFe12.0–x (Nb0.5Zn0.5) xO19. J. Alloys Compds. **765**, 616–623 (2018)
19. S. Simpson, S. Fop, H.A. Hopper, G.B.G. Stenning, C. Ritter, A.C. McLaughlin, Electronic phase separation in the hexagonal perovskite Ba3SrMo2. Phys. Rev. Mater. **6**(2), 024401 (2022)
20. D. Klygach, M. Vakhitov, D. Vinnik, A. Bezborodov, S. Gudkova, V. Zhivulin, D. Zherebtsov, C. SakthiDharan, S. Trukhanov, A. Trukhanov, Measurement of permittivity and permeability of barium hexaferrite. J. Magn. Magn. Mater. **465**, 290–294 (2018)
21. A. Trukhanov, V. Kostishyn, L. Panina, V. Korovushkin, V. Turchenko, P. Thakur, A. Thakur, Y. Yang, D. Vinnik, E. Yakovenko, Control of electromagnetic properties in substituted M-type hexagonal ferrites. J. Alloy. Compd. **754**, 247–256 (2018)
22. M.A. Almessiere, A.V. Trukhanov, Y. Slimani, K. You, S.V. Trukhanov, E.L. Trukhanova, F. Esa, A. Sadaqat, K. Chaudhary, M. Zdorovets, Correlation between composition and electrodynamics properties in nanocomposites based on hard/soft ferrimagnetics with strong exchange coupling. Nanomaterials **9**(2), 202 (2019)
23. S. Trukhanov, A. Trukhanov, V. Kostishyn, L. Panina, A.V. Trukhanov, V. Turchenko, D. Tishkevich, E. Trukhanova, O. Yakovenko, L.Y. Matzui, Investigation into the structural features and microwave absorption of doped barium hexaferrites. Dalton Trans. **46**(28), 9010–9021 (2017)
24. D. Vinnik, V. Zhivulin, A.Y. Starikov, S. Gudkova, E. Trofimov, A. Trukhanov, S. Trukhanov, V. Turchenko, V. Matveev, E. Lahderanta, Influence of titanium substitution on structure, magnetic

and electric properties of barium hexaferrites BaFe12− xTixO19. J. Magn. Magn. Mater. **498**, 166117 (2020)
25. C. Fang, F. Kools, R. Metselaar, R. De Groot, Magnetic and electronic properties of strontium hexaferrite SrFe12O19 from first-principles calculations. J. Phys. Condens. Matter **15**(36), 6229 (2003)
26. S.A. Mathews, D.R. Babu, Analysis of the role of M-type hexaferrite-based materials in electromagnetic interference shielding. Curr. Appl. Phys. **29**, 39–53 (2021)
27. G. Todkar, R. Kunale, R. Kamble, K.M. Batoo, M. Ijaz, A. Imran, M. Hadi, E. Raslan, S.E. Shirsath, R. Kadam, Ce–Dy substituted barium hexaferrite nanoparticles with large coercivity for permanent magnet and microwave absorber application. J. Phys. D **54**(29), 294001 (2021)
28. E.-S. Lim, H.K. Kim, Y.-M. Kang, Control of electromagnetic wave absorption properties in La-Co-Ti substituted M-type hexaferrite–epoxy composites. J. Magn. Magn. Mater. **517**, 167397 (2021)
29. K.S. Ounnunkad, P. Winotai, S. Phanichphant, Effect of La doping on structural, magnetic and microstructural properties of Ba 1–x La x Fe 12 O 19 ceramics prepared by citrate combustion process. J. Electroceram. **16**, 357–361 (2006)
30. A. Baykal, I. Auwal, S. Güner, H. Sözeri, Magnetic and optical properties of Zn2+ ion substituted barium hexaferrites. J. Magn. Magn. Mater. **430**, 29–35 (2017)
31. X. Obradors, A. Collomb, M. Pernet, J. Joubert, A. Isalgué, Structural and magnetic properties of BaFe12−xMnxO19 hexagonal ferrites. J. Magn. Magn. Mater. **44**(1–2), 118–128 (1984)
32. A. Kumar, studies on dielectric, electrical & magnetic properties of Co and Ni-doped barium hexaferrite (BaFe12O19). IIT (BHU) Varanasi (2020)
33. J. Ahmad, A.R. Makhdoom, M. Sabir, S.U. Asif, M.Q. Awan, Electrical transport properties of cobalt-doped MgAl2O4 nanoparticles. Phys. Scr. **94**(10), 105814 (2019)
34. A.R. Makhdoom, Q.A. Ranjha, U.-u-R. Ghori, M.A. Raza, B. Raza, M.E. Mazhar, K.A. Rao, F. Ahmed, S.U. Asif, M.W. Khan, M. Nisa, Structural and magnetic variations in Ba05Sr-05Fe9Ce1Al2O19 hexaferrites at different sintering temperatures. Phys. Scr. **96**(12), 125865 (2021)
35. A.R. Makhdoom, F. Ahmed, U.U. Ghori, Q.A. Ranjha, K.A. Rao, A. Javed, M.E. Mazhar, M. Bukhari, A. Maqsood, S.U. Asif, M.W. Khan, Tuning magnetic properties in the Ce–Al Co-substituted M-type BaSr (6: 4) hexaferrites. J. Mater. Sci. Mater. Electron. **33**(9), 7266–74 (2022)
36. A. Makhdoom, F. Ahmed, U.-u-R. Ghori, Q.A. Ranjha, K.A. Rao, A. Javed, M.E. Mazhar, M. Bukhari, A. Maqsood, S.U. Asif, Tuning magnetic properties in the Ce–Al Co-substituted M-type BaSr (6: 4) hexaferrites. J. Mater. Sci.: Mater. Electron. **33**(9), 7266–7274 (2022)
37. K.M.U. Rehman, X. Liu, S. Feng, Y. Yang, J. Tang, W. Wei, Z. Wazir, M.W. Khan, C. Zhang, C. Liu, Synthesis of Sr .7YxLa .3−xFe12− y CoyO19 (x= 0.00, 0.05, 0.10, 0.15) & (y= 0.30, 0.25, 0.20, 0.15) hexaferrites against structures and magnetic properties prepared by the solid-state reaction method. Chin. J. Phys. **55**(5), 1780–1786 (2017)
38. S. Trukhanov, A. Trukhanov, V. Turchenko, A.V. Trukhanov, E. Trukhanova, D. Tishkevich, V. Ivanov, T. Zubar, M. Salem, V. Kostishyn, Polarization origin and iron positions in indium doped barium hexaferrites. Ceram. Int. **44**(1), 290–300 (2018)
39. S. Trukhanov, A. Trukhanov, V. Turchenko, V. Kostishin, L. Panina, I. Kazakevich, A. Balagurov, Crystal structure and magnetic properties of the BaFe12− xInxO19 (x= 0.1–1.2) solid solutions. J. Magn. Magn. Mater. **417**, 130–136 (2016)
40. M.K. Bilal, J. Wang, R. Bashir, H. Liu, S.U. Asif, J. Xie, W. Hu, A novel relaxor (Bi, Na, Ba)(Ti, Zr) O3 lead-free ceramic with high energy storage performance. J. Am. Ceram. Soc. **104**(8), 3982–3991 (2021)
41. S.U. Asif, J. Wang, Y. Qian, D. Gao, R. Bashir, M.K. Bilal, J. Ahmad, M.Q. Awan, W. Hu, Phonon vibrations and photoluminescence emissions and their correlations with the electrical properties in Er3+ doped Bi3YO6 oxide-ion conductors. Solid State Ionics **344**, 115092 (2020)
42. M. Shezad, X. Liu, S. Feng, X. Kan, W. Wang, C. Liu, T.J. Shehzad, K.M.U. Rehman, Characterizations analysis of magneto-structural transitions in Ce-Co doped SrM based nano Sr1− xCexFe12− xCoxO19 hexaferrite crystallites prepared by ceramic route. J. Magn. Magn. Mater. **497**, 166013 (2020)
43. B.H. Alshammari, U.-u-R. Ghori, Q.A. Ranjha, S. Ahmad, W. Abbas, S.U. Asif, F. Ahmed, F.A. Ibrahim, M.S. Hamdy, S.M. Eldin, Structural and magnetic conduct in Sm and Al substituted Ba09Sm 01 Fe10Al2O19 M-type hexaferrites at different sintering temperatures. Phys. Scr. **98**, 065905 (2023)
44. B. Wen, J. Zhao, T. Li, C. Dong, n-diamond: an intermediate state between rhombohedral graphite and diamond? New J. Phys. **8**(5), 62 (2006)
45. H. Hirai, K.I. Kondo, H. Sugiura, Possible structural models of n-diamond: a modified form of diamond. Appl. Phys. Lett. **61**(4), 414–416 (1992)
46. Y. He, Y.-L. Hou, Y.-L. Wong, R. Xiao, M.-Q. Li, Z. Hao, J. Huang, L. Wang, M. Zeller, J. He, Z. Xu, Improving stability against desolvation and mercury removal performance of Zr(iv)–carboxylate frameworks by using bulky sulfur functions. J. Mater. Chem. A **6**(4), 1648–1654 (2018)
47. C. Liu, X. Kan, F. Hu, X. Liu, S. Feng, J. Hu, W. Wang, K.M.U. Rehman, M. Shezad, C. Zhang, H. Li, S. Zhou, Q. Wu, Investigations of Ce-Zn co-substitution on crystal structure and ferrimagnetic properties of M-type strontium hexaferrites Sr1−xCexFe12−xZnxO19 compounds. J. Alloy Compd. **785**, 452–459 (2019)
48. S. Anand, S. Pauline, V.M. Vinosel, M.A. Janifer, Structural rietveld refinement and vibrational study of M-type BaFe12O19 nanoparticles. Mater. Today Proc. **8**, 476–483 (2019)
49. K.M.U. Rehman, X. Liu, M. Li, S. Jiang, Y. Wu, C. Zhang, C. Liu, X. Meng, H. Li, Synthesization and magnetic properties of Ba1−xYxFe12O19 hexaferrites prepared by solid-state reaction method. J. Magn. Magn. Mater. **426**, 183–187 (2017)
50. M.S. Shifa, W.A. Khan, H. Albalawi, T.I. Al-Muhimeed, A.A. AlObaid, Q. Mahmood, M.A. Khan, S. Gulbadan, Z.A. Gilani, I. Qureshi, Effects of heat treatment on the structural, spectral, morphological, dielectric, and magnetic properties of Ba0.5Sr0.1Zn0.4Fe12O19 ferrite. Ceram. Int. **47**(17), 24817–22 (2021)
51. M.M.L. Sonia, S. Anand, V.M. Vinosel, M.A. Janifer, S. Pauline, A. Manikandan, Effect of lattice strain on structure, morphology and magneto-dielectric properties of spinel NiGdxFe2− xO4 ferrite nano-crystallites synthesized by sol-gel route. J. Magn. Magn. Mater. **466**, 238–251 (2018)
52. M.M.L. Sonia, S. Anand, V.M. Vinosel, M. Asisi Janifer, S. Pauline, Effect of lattice strain on structural, magnetic and dielectric properties of sol–gel synthesized nanocrystalline Ce 3+ substituted nickel ferrite. J. Mater. Sci.: Mater. Electron. **29**, 15006–15021 (2018)
53. H. Irfan, K.M. Racik, S. Anand, Microstructural evaluation of CoAl2O4 nanoparticles by Williamson-Hall and size–strain plot methods. J. Asian Ceram. Soc. **6**(1), 54–62 (2018)
54. S.U. Asif, S. Rizwan, M.Q. Awan, M.W. Khan, I. Sadiq, M.E. Mazhar, A. Ahmad, S.S. Hussain, E.U. Khan, W. Hu, M.N. Ashiq, Effect of Dy-Co on physical and magnetic properties of X-type hexaferrites (Ba2−xDyxCu2Fe28−yCoyO46). Chin. J. Phys. **61**, 47–54 (2019)

55. M.Q. Awan, J. Ahmad, A. Waheed, S.A.R. Gillani, F. Ahmed, S.U. Asif, M.E. Mazhar, S. Anwar, Facile synthesis and characterizations of Co2+ doped Bi0.8Ba0.2FeO3 nano-crystalline multiferroic ceramics. Phys. Scr. **96**(10), 5805 (2021)
56. H.M. Khan, M. Islam, Y. Xu, M.A. Iqbal, I. Ali, Structural and magnetic properties of TbZn-substituted calcium barium M-type nano-structured hexa-ferrites. J. Alloy Compd. **589**, 258–262 (2014)
57. M.E. Mazhar, S. Bakhtawar, A.M. Rana, M. Nauman Usmani, N. Akhtar, W. Abbas, K. Khan, J. Ahmad, Insight into the structural characterization of pure and Zr-doped hydrothermally synthesized cerium oxide nanoparticles. Mater. Res. Express. **6**(10), 105022 (2019)
58. M.K. Bilal, R. Bashir, S.U. Asif, J. Wang, W. Hu, Enhanced energy storage properties of 0.7Bi0.5Na0.5TiO3–0.3SrTiO3 ceramic through the addition of NaNbO3. Ceram. Int. **47**(21), 1–20 (2021)
59. J. Lee, E.J. Lee, T.-Y. Hwang, J. Kim, Y.-H. Choa, Anisotropic characteristics and improved magnetic performance of Ca–La–Co-substituted strontium hexaferrite nanomagnets. Sci. Rep. **10**(1), 15929 (2020)
60. K.S. Martirosyan, E. Galstyan, S.M. Hossain, Y.-J. Wang, D. Litvinov, Barium hexaferrite nanoparticles: synthesis and magnetic properties. Mater. Sci. Eng. B **176**(1), 8–13 (2011)
61. M. Shezad, X. Liu, S. Feng, X. Kan, W. Wang, C. Liu, T.J. Shehzad, K.M.U. Rehman, Characterizations analysis of magneto-structural transitions in Ce-Co doped SrM based nano Sr1−xCexFe12−xCoxO19 hexaferrite crystallites prepared by ceramic route. J. Magn. Magn. Mater. **497**, 166013 (2020)
62. D. Shekhawat, P. Roy, Effect of cobalt substitution on physical & electro-magnetic properties of SrAl4Fe8O19 hexa-ferrite. Mater. Chem. Phys. **229**, 183–189 (2019)
63. A. Trukhanov, L. Panina, S. Trukhanov, V. Turchenko, I. Kazakevich, M. Salem, Features of crystal structure and magnetic properties of M-type Ba-hexaferrites with diamagnetic substitution. Int. J. Mater. Chem. Phys. **1**, 286–294 (2015)
64. A. Makhdoom, Q. Ranjha, U.-u-R. Ghori, M. Raza, B. Raza, M.E. Mazhar, K. Rao, F. Ahmed, S.U. Asif, M. Khan, M. Nisa, Structural and magnetic variations in Ba 05 Sr 05 Fe 9 Ce 1 Al 2 O 19 hexaferrites at different sintering temperatures. Phys. Scr. **96**, 125865 (2021)
65. V. Turchenko, A. Balagurov, S. Trukhanov, A. Trukhanov, Refinement of the atomic and magnetic structures of solid solutions BaFe12 – xInxO19 (x = 01–12) by the neutron diffraction method. J. Surf. Invest. **13**, 69–81 (2019)